

# Thermoelastic effect from an atomistic perspective

Matthew Kiener and Mihir Sen

*Department of Aerospace and Mechanical Engineering  
University of Notre Dame, Notre Dame, IN 46556*

October 26, 2011

## Abstract

The quasi-static deformation of a single atom system is considered to assess the fundamental causes of the thermoelastic effect (TEE) on an atomistic scale. Two models of deformation are employed. The first, Model 1, consists of a force applied to an atom bounded by the Lennard-Jones potential. The second, Model 2, consists of the prescribed motion of an atom adjacent to the atom of interest. Two mechanisms are considered as possible causes of the TEE. The first, Mechanism 1, states that the oscillation energy of the atom, i.e. the maximum kinetic energy, changes throughout deformation. The second, Mechanism 2, states that the partition of the oscillation energy shifts throughout deformation, leading to a change in the time average of the kinetic energy. Analysis utilizing approximations of the quasi-static deformation is performed and verified via numerical simulations to demonstrate that Mechanism 1, caused by the decreasing concavity of the Lennard-Jones potential, is compatible with the TEE for both models. A numerical method is used to demonstrate that Mechanism 2 is compatible with the TEE for Model 1 but not Model 2. As such, it is concluded that Mechanism 1 and the decreasing concavity of the Lennard-Jones potential are responsible for the TEE. The numerical simulations for each model reveal some characteristics of the TEE over a range of oscillation energies and deformations.

## I. INTRODUCTION

The thermoelastic effect (TEE) is the change in temperature of a solid upon deformation. For a solid with a positive coefficient of thermal expansion, compression increases the temperature and extension decreases the temperature. This effect is well known from a macroscopic perspective, both experimentally and thermodynamically. In contrast, the TEE is less understood from an atomistic perspective, in which the

solid is viewed as a collection of nonlinear oscillators. These two scales are related by

$$\bar{K} = \frac{D}{2}k_B T, \quad (1)$$

where  $\bar{K}$  is the average kinetic energy per atom of the comprising atoms,  $D$  is the number of spatial dimensions in the system,  $k_B$  is the Boltzmann constant, and  $T$  is the temperature of the macroscopic object. From the discrete perspective, the TEE implies that compressional deformation increases  $\bar{K}$  for a system of atomic oscillators, whereas extensional deformation decreases it. This dependence of the sign of change in kinetic energy on the type of deformation deserves some explanation.

There have been several attempts in recent years to demonstrate and explain the TEE from an atomistic perspective.<sup>1-3</sup> Each of these attempts considered the deformation of a single anharmonic oscillator, the basic element of a solid. A basic justification of this approach is that properties of a collection of oscillators can be reduced to that of a single oscillator by assuming a model of statistically independent oscillating particles.<sup>3</sup> This study will also consider the deformation of a single oscillator in order to extend the results of these previous studies and to provide new insights into the TEE. In addition to utilizing a model similar to that in the previous works, it will also employ a new model. Furthermore, this study will consider two possible mechanisms of the TEE for both of these models.

## II. MODELS

The atomic bond will be modeled using the Lennard-Jones pair potential. Shown in Fig. 1, this potential is given by

$$U_{LJ}(r) = 4\epsilon \left[ \left( \frac{\sigma}{r} \right)^{12} - \left( \frac{\sigma}{r} \right)^6 \right] + \epsilon, \quad (2)$$

where  $r$  is the spacing between atoms and  $\epsilon$  and  $\sigma$  are bond parameters. The equilibrium spacing of the bond is given by  $R = 2^{1/6}\sigma$ . This potential was chosen since it is often used in studies concerned with qualitative properties of materials. The previous studies used a cubic potential, which comparatively has a smaller applicable range for the energy of the oscillator as well as the deformation. From this point forward, the potential will be denoted generally as  $U_1(r)$ , since many of the equations used are not restricted to the Lennard-Jones potential.

The first model of deformation of a single atomic oscillator is shown in Fig. 2. This is the same model employed by the previous studies and will be referred to as Model 1. The left atom is fixed, and the right atom is free to oscillate. A time-dependent force  $F(t)$  is exerted on the mass to simulate deformation. For extensional deformation,  $F > 0$ , and for compressional deformation,  $F < 0$ . The deformation is assumed to be quasi-static, i.e. there are no changes in the kinetic energy of the oscillator due to dynamic effects. This requires that  $\left|\frac{dF}{dt}\right|$  is small relative to the oscillator dynamics.

The second model of deformation is shown in Fig. 3. This model has not yet been studied and will be referred to as Model 2. The left atom is fixed, the center atom is free to oscillate, and the right atom is given a prescribed motion  $x_r(t)$  to simulate deformation. For extensional deformation,  $\frac{dx_r}{dt} > 0$ , and for compressional deformation,  $\frac{dx_r}{dt} < 0$ . The deformation is also quasi-static, implying  $\left|\frac{dx_r}{dt}\right|$  is relatively small.

Further details and restrictions of the two models will be described in their corresponding sections.

### III. ENERGY CHARACTERISTICS AND MECHANISMS OF THE TEE

The energy characteristics of each model are described in the same way. In each

model, the oscillating mass is bound in an overall time-dependent potential well  $U(r, t)$ . The time-dependence is due to the deformation. Since the deformation is assumed to be quasi-static, the well shape changes at a much slower rate than the oscillation of the mass. A schematic of an arbitrary time-dependent potential well with only one minimum is shown in Fig. 4. The mass oscillates between the lower and upper bounds  $r_l$  and  $r_r$ , respectively. The total energy of the system is given by

$$E_{tot} = E_{osc} + U_s, \quad (3)$$

where  $E_{osc}$  is the oscillation energy and  $U_s$  is the static potential energy. The static potential energy is the potential energy due to the deformation of the system. For an undeformed system,  $U_s = 0$ . The oscillation energy is given by

$$E_{osc} = K + U_d, \quad (4)$$

where  $K$  is the kinetic energy and  $U_d$  is the dynamic potential energy. These two quantities exchange back and forth with each other as the mass oscillates. It is clear that  $E_{osc} = K_{max}$ , which is the kinetic energy at the well minimum. The total potential energy is given by  $U = U_d + U_s$ .

With these defined quantities, there are two possible mechanisms responsible for the TEE. The first mechanism, which will be referred to as Mechanism 1, is that the magnitude of  $E_{osc}$  changes during deformation, thus affecting the value of  $K$ . This mechanism implies that deformation morphs the overall well in a way that changes the depth of the well occupied by the oscillator. The following derives an expression that can be used to evaluate this mechanism. Rewriting the quantities in Eq. (4)

yields

$$E_{osc}(t) = \frac{1}{2}mv(t)^2 + U(r(t), t) - U(r_{min}(t), t), \quad (5)$$

where  $m$  is the mass,  $v$  is the mass's velocity,  $r$  is its position, and  $r_{min}$  is the location of the minimum of the potential well. This is given by  $\frac{\partial U}{\partial r}|_{(r_{min}, t)} = 0$ . Taking the derivative with respect to time yields

$$\frac{dE_{osc}}{dt} = mv \frac{dv}{dt} + \left( \frac{\partial U}{\partial r} \Big|_{(r,t)} \frac{dr}{dt} + \frac{\partial U}{\partial t} \Big|_{(r,t)} \right) - \left( \frac{\partial U}{\partial r} \Big|_{(r_{min}, t)} \frac{dr_{min}}{dt} + \frac{\partial U}{\partial t} \Big|_{(r_{min}, t)} \right). \quad (6)$$

The first two terms cancel out and the fourth term is identically zero, which yields

$$\frac{dE_{osc}}{dt} = \frac{\partial U}{\partial t} \Big|_{(r,t)} - \frac{\partial U}{\partial t} \Big|_{(r_{min}, t)}. \quad (7)$$

This equation is a continuous extension of the results of an earlier study.<sup>3</sup> This study considered an infinitesimal step force applied to the mass, and it concluded that the oscillation energy would increase if the well minimum decreases, and vice-versa. Similarly, this equation implies that  $E_{osc}$  increases if the potential well is increasing more at  $r$  than at  $r_{min}$ . If the well is time-independent,  $\frac{\partial U}{\partial r} \Big|_{(r,t)} = 0$  for all values of  $r$ , and thus  $E_{osc}$  is constant, as expected. This equation will later be applied to each model to assess whether  $E_{osc}$  changes over the course of deformation.

The second possible mechanism, which will be referred to as Mechanism 2, is that the partition of energy within  $E_{osc}$  (i.e.  $K$  and  $U_d$ ) shifts during deformation. More specifically, the time averages of  $K$  and  $U_d$  over a period of oscillation, denoted by  $\langle K \rangle$  and  $\langle U_d \rangle$ , change over the course of deformation. This mechanism implies that deformation changes the shape of the well occupied by the oscillator in a way that contributes to a change in  $K$ . A general expression for  $\langle K \rangle$  for a given well shape

and a given value of  $E_{osc}$  is obtained as follows. Integrating  $K$  over half of the period yields

$$\langle K \rangle = \frac{2}{T} \int_0^{T/2} K dt. \quad (8)$$

Since  $r(t)$  cannot in general be determined, the integral over time must be converted to an integral over space, which can be calculated using the overall potential. Using

$$\frac{dr}{dt} = \sqrt{\frac{2}{m}} \sqrt{K}, \quad (9)$$

the expressions in Eq. (8) can be evaluated as

$$\int_0^{T/2} K dt = \int_{r_l}^{r_r} \frac{K}{\frac{dr}{dt}} dr = \sqrt{\frac{m}{2}} \int_{r_l}^{r_r} \sqrt{K} dr \quad (10)$$

and

$$\frac{T}{2} = \sqrt{\frac{m}{2}} \int_{r_l^+}^{r_r^-} \frac{1}{\sqrt{K}} dr. \quad (11)$$

Notice this last equation is a double-sided improper integral since  $K|_{r_l} = K|_{r_r} = 0$ . The notation  $r_l^+$  and  $r_r^-$  is used to represent the approaching limit from the positive side of  $r_l$  and the negative side of  $r_r$ , respectively. It can be argued that this and all subsequent improper integrals converge from a physical basis. Substituting these two results into Eq. (8) yields

$$\langle K \rangle = \frac{\int_{r_l^+}^{r_r^-} \sqrt{K} dr}{\int_{r_l^+}^{r_r^-} \frac{1}{\sqrt{K}} dr}. \quad (12)$$

This equation will later be applied to each model to assess whether  $\langle K \rangle$  shifts over

the course of deformation.

With the two models of deformation and the two possible mechanisms of the TEE, there are four cases to consider. The two models will be considered sequentially, and within each model the two mechanisms will be considered.

#### IV. MODEL 1

Before each mechanism is considered, some further details and restrictions concerning this model will now be described. The overall well is given by  $U(r, t) = U_1(r) - F(t)(r - r_{min}(t))$ . The constant of integration  $F r_{min}$  was chosen so that  $U(r_{min}, t) = U_1(r_{min})$ . This makes the static potential energy in the overall well physically meaningful. The imposed restrictions on the model are as follows. For  $F < 0$ , there are no restrictions on the magnitude of  $F$  since a single local minimum will be present in the overall well for any value. There is also no restriction on  $E_{osc}$  for this case: the oscillator will remain bounded for any value of  $E_{osc}$  since both walls of the overall potential well approach infinity. On the other hand, there are restrictions for both of these quantities for  $F > 0$ . The magnitude of  $F$  must satisfy  $F < \left. \frac{dU_1}{dr} \right|_{r_i}$ , where  $r_i$  is the inflection point in the Lennard-Jones well. Otherwise the overall well has no minimum and the oscillator will be unbounded for any value of  $E_{osc}$ . Assuming this is satisfied, the value of  $E_{osc}$  still must be less than a critical value since the well has a local maximum to the right of the minimum. This critical value is the difference in the overall potential at the local maximum and the local minimum.

##### A. Mechanism 1

###### 1. Analysis

Equation (7) will now be applied to this model to assess the contribution of Mechanism 1 to the TEE. Taking the partial derivative of  $U(r, t)$  with respect to time

yields

$$\left. \frac{\partial U}{\partial t} \right|_{(r,t)} = -\frac{dF}{dt}r + \frac{dF}{dt}r_{min} + F\frac{dr_{min}}{dt}. \quad (13)$$

Substituting this expression into Eq. (7) yields

$$\frac{dE_{osc}}{dt} = \frac{dF}{dt} [r_{min}(t) - r(t)]. \quad (14)$$

From this, since  $r(t)$  oscillates,  $E_{osc}$  will also oscillate. Therefore, this equation must be averaged over time to compute to average value of  $\frac{dE_{osc}}{dt}$  at a given point in the deformation. For quasi-static deformation, it will be assumed that  $\frac{dF}{dt} = \mu$  (i.e. constant over the course of deformation). Furthermore, it will be assumed that  $F(t) = F$  and thus  $r_{min}(t) = r_{min}$  over a period of oscillation of the mass. Taking into account the above approximations and averaging Eq. (14) over half of the period yields

$$\left\langle \frac{dE_{osc}}{dt} \right\rangle_{F,E_{osc}} = \frac{2\mu}{T} \int_0^{T/2} r_{min} - r(t) dt. \quad (15)$$

Converting the integral over time to one over space in a way similar to that done earlier for  $\langle K \rangle$  yields

$$\left\langle \frac{dE_{osc}}{dt} \right\rangle_{F,E_{osc}} = \mu \frac{\int_{r_l^+}^{r_r^-} \frac{r_{min}-r}{\sqrt{K}} dr}{\int_{r_l^+}^{r_r^-} \frac{1}{\sqrt{K}} dr}. \quad (16)$$

For Mechanism 1 to contribute to the TEE, Eq. (16) has simple requirements: it is necessary that  $\left\langle \frac{dE_{osc}}{dt} \right\rangle_{F,E_{osc}} > 0$  for compressional deformation and  $\left\langle \frac{dE_{osc}}{dt} \right\rangle_{F,E_{osc}} < 0$  for extensional deformation. Since the denominator of Eq. (16) is positive and  $\mu > 0$  and  $\mu < 0$  for extensional and compressional deformation, respectively, the integral in the numerator of Eq. (16) (denote it as  $I_1$ ) must be negative for the TEE to exist.

Notice that Eq. (16) describes the TEE *at the given value of  $F$  and the given value of  $E_{osc}$* , which only gives information about one point during the course of deformation. To determine how  $E_{osc}$  behaves throughout the entire deformation,  $\left\langle \frac{dE_{osc}}{dt} \right\rangle_{F, E_{osc}}$  must be integrated over the course of deformation.

The dependence of  $\left\langle \frac{dE_{osc}}{dt} \right\rangle$  on  $F$  and  $E_{osc}$  raises some interesting questions. For example, is it possible that  $E_{osc}$  will be increasing at one point during the deformation and then decreasing at another? Will the overall change in  $E_{osc}$  depend upon its initial value? So these problematic cases do not occur, it is necessary that  $I_1 < 0$  for all values of  $F$  and  $E_{osc}$ . This will cause  $E_{osc}$  to increase and decrease monotonically over the course of compressional and extensional deformation, respectively, for any initial value of  $E_{osc}$ . It will now be shown that this is indeed the case for the Lennard-Jones potential.

Separating  $I_1$  into two intervals, substituting  $\Delta r = r - r_{min}$ , and defining  $\Delta r_r = r_r - r_{min}$  and  $\Delta r_l = r_{min} - r_l$  yields

$$I_1 = \left[ - \int_{-\Delta r_l^+}^0 \frac{\Delta r}{\sqrt{K}|\Delta r + r_{min}|} d\Delta r \right] - \left[ \int_0^{\Delta r_r^-} \frac{\Delta r}{\sqrt{K}|\Delta r + r_{min}|} d\Delta r \right]. \quad (17)$$

Rewriting the first term in this expression using the substitution  $\Delta r^* = -\Delta r$  yields

$$\int_0^{\Delta r_l^-} \frac{\Delta r^*}{\sqrt{K}|\Delta r^* + r_{min}|} d\Delta r^*. \quad (18)$$

Before the second integral is considered, an important property of the Lennard-Jones potential will be considered. It is given by the following inequality:

$$\left. \frac{dU}{dr} \right|_r = \int_{r_{min}}^r \frac{d^2 U}{dr^2} dr = \int_{r_{min}}^r \frac{d^2 U_1}{dr^2} dr < \int_{r_{min}}^r \left. \frac{d^2 U_1}{dr^2} \right|_{r_{min}} dr = \left. \frac{d^2 U_1}{dr^2} \right|_{r_{min}} (r - r_{min}). \quad (19)$$

This inequality is due to “bond-softening”, or decreasing concavity:  $\left.\frac{d^2 U_1}{dr^2}\right|_{r_{min}} > 0$  (imposed by the previously stated restrictions) and  $\frac{d^2 U_1}{dr^2}$  monotonically decreases until it reaches its minimum negative value, at which point it increases asymptotically towards zero. This makes  $\frac{d^2 U_1}{dr^2} < \left.\frac{d^2 U_1}{dr^2}\right|_{r_{min}}$  on  $r > r_{min}$  and  $\frac{d^2 U_1}{dr^2} > \left.\frac{d^2 U_1}{dr^2}\right|_{r_{min}}$  on  $r < r_{min}^1$ , hence the inequality.

Now the following expression will be considered:

$$E_{osc} = \int_0^{\Delta r_r} \left.\frac{dU}{dr}\right|_{\Delta r+r_{min}} d\Delta r = \int_0^{\Delta r_l} \left.-\frac{dU}{dr}\right|_{-\Delta r^*+r_{min}} d\Delta r^*. \quad (20)$$

Substituting Eq. (19) into the first term above yields

$$E_{osc} < \frac{1}{2} \left.\frac{d^2 U_1}{dr^2}\right|_{r_{min}} \Delta r_r^2. \quad (21)$$

Substituting Eq. (19) into the second term above yields

$$E_{osc} > \frac{1}{2} \left.\frac{d^2 U_1}{dr^2}\right|_{r_{min}} \Delta r_l^2. \quad (22)$$

Since both  $\Delta r_r$  and  $\Delta r_l$  are positive, the above expression can be combined to yield  $\Delta r_l < \Delta r_r$ . Since this holds for any allowable value of  $E_{osc}$ , a function  $\zeta$  can be defined by  $\Delta r = \Delta r^* + \zeta(\Delta r^*)$ , where  $\Delta r \in [0, \Delta r_r]$ ,  $\Delta r^* \in [0, \Delta r_l]$ ,  $\zeta > 0$  for  $\Delta r^* > 0$ , and  $\zeta = 0$  for  $\Delta r^* = 0$ . In other words, the function  $\Delta r^* + \zeta(\Delta r^*)$  maps the interval  $[0, \Delta r_l]$  to  $[0, \Delta r_r]$  in a one to one fashion, where corresponding points have the same potential energy, or equivalently the same kinetic energy:  $K|_{\Delta r^*+\zeta(\Delta r^*)+r_{min}} = K|_{-\Delta r^*+r_{min}}$ .

Returning to Eq. (17), substituting  $\Delta r = \Delta r^* + \zeta(\Delta r^*)$  into the second term yields

$$\int_0^{\Delta r_l^-} \frac{(\Delta r^* + \zeta(\Delta r^*)) \left(1 + \frac{d\zeta}{d\Delta r^*}\right)}{\sqrt{K|_{\Delta r^*+\zeta(\Delta r^*)+r_{min}}}} d\Delta r^*. \quad (23)$$

Recombining the two integrals in Eq. (17) yields

$$I_1 = \int_0^{\Delta r_l^-} \frac{\Delta r^* - (\Delta r^* + \zeta(\Delta r^*)) \left(1 + \frac{d\zeta}{d\Delta r^*}\right)}{\sqrt{K}|_{\Delta r^* + \zeta(\Delta r^*) + r_{min}}} d\Delta r^*. \quad (24)$$

It will now be shown why the above integral must be negative. Substituting  $\Delta r = \Delta r^* + \zeta(\Delta r^*)$  into the first integral in Eq. (20) yields

$$E_{osc} = \int_0^{\Delta r_l} \frac{dU}{dr} \Big|_{\Delta r^* + \zeta(\Delta r^*) + r_{min}} \left(1 + \frac{d\zeta}{d\Delta r^*}\right) d\Delta r^* = \int_0^{\Delta r_l} -\frac{dU}{dr} \Big|_{-\Delta r^* + r_{min}} d\Delta r^*. \quad (25)$$

Taking the derivative with respect to  $\Delta r_l$  yields

$$\frac{dE_{osc}}{d\Delta r_l} = \frac{dU}{dr} \Big|_{\Delta r_l + \zeta(\Delta r_l) + r_{min}} \left(1 + \frac{d\zeta}{d\Delta r^*} \Big|_{\Delta r_l}\right) = -\frac{dU}{dr} \Big|_{-\Delta r_l + r_{min}}. \quad (26)$$

Applying Eq. (19) yields

$$1 + \frac{d\zeta}{d\Delta r^*} \Big|_{\Delta r_l} > \frac{\Delta r_l}{\Delta r_l + \zeta(\Delta r_l)} > 0. \quad (27)$$

Since this holds for any  $\Delta r_l$ , it can be substituted into Eq. (24) to yield

$$I_1 < \int_0^{\Delta r_l^-} \frac{\Delta r^* - (\Delta r^* + \zeta(\Delta r^*)) \frac{\Delta r^*}{\Delta r^* + \zeta(\Delta r^*)}}{\sqrt{K}|_{\Delta r^* + \zeta(\Delta r^*) + r_{min}}} d\Delta r^* = 0. \quad (28)$$

Notice that this holds true for all allowable values of  $E_{osc}$  in addition to all values of  $F$  such that  $\frac{d^2 U_1}{dr^2} \Big|_{r_{min}} > 0$ , which was imposed so a local minimum exists in the well. Given this, the “local” TEE for this system exists at all points over the course of deformation, meaning that indeed  $E_{osc}$  changes monotonically over deformation. This result was all due to the monotonic<sup>2</sup> “bond softening” of the Lennard-Jones

well. If the well “hardened” in some places, e.g. at some point to the right of the minimum, the TEE would be “backwards” in the vicinity of this point, meaning that  $E_{osc}$  would not change monotonically over the course of deformation.

## 2. Simulation

The results of the above analysis were verified by two methods of simulation. First, the equations of motion were numerically integrated. Second, Eq. (16) was numerically evaluated to demonstrate compatibility with the other simulation results.

The system was simulated for parameter values corresponding to solid argon:  $\epsilon/k_B = 120$  K,  $\sigma = 3.4$  Å, and  $m = 39.9$  amu.<sup>4</sup> Initial oscillation energies of  $10Kk_B$  to  $40Kk_B$  were used in order to approximate initial “temperature”<sup>3</sup> values of 10 K to 40 K by assuming  $\langle K \rangle \approx E_{osc}/2$ . The values of strain, defined as  $\epsilon_s = (r_{min_f} - R)/R$ , where  $r_{min_f} = r_{min}(t_f)$ , ranged from -0.03 to 0.03<sup>4</sup>.

The quasi-static deformation was modeled as a sigmoid. The force ranges from 0 to  $F$  over the interval  $[0, t_f]$ . The sigmoid is given by a fourth order polynomial over this interval, where the five constants were determined such that  $F(0) = 0$ ,  $\dot{F}(0) = 0$ ,  $F(t_f/2) = F/2$ ,  $F(t_f) = F$ , and  $\dot{F}(t_f) = 0$ . Quasi-static deformation was imposed by specifying  $\left(\frac{dF}{dt}\right)_{max} = \frac{dF}{dt}\Big|_{t_f/2} \approx 10^{-2} \cdot F/t_{osc}$ , where  $t_{osc}$  is the approximated characteristic period of oscillation of a mass. It is given by

$$t_{osc} = \frac{2\pi}{\sqrt{k_{lin}/m}}, \quad (29)$$

where  $k_{lin} = 72\epsilon/2^{1/3}\sigma^2$  is the equivalent linear elastic force constant of a single Lennard-Jones bond about its equilibrium position. The value of  $\frac{dF}{dt}\Big|_{t_f/2}$  was conservatively approximated to be  $2F/t_f$ . The two expressions were equated, yielding  $t_f = 2 \cdot 10^2 t_{osc}$ .

To simulate the system, the initial conditions were determined based on the ini-

tial oscillation energy. The equations of motion were integrated using a fifth order Gear Predictor-Corrector scheme over the course of deformation. This is a common scheme for molecular dynamics simulations since it is energy conservative. The energy characteristics of the system were monitored throughout the deformation.

The results of an extensional simulation and a compressional simulation demonstrating the TEE are shown in Fig. 5 to Fig. 8. Since  $K_{max} = E_{osc}$ , it is clear from Fig. 5 that  $E_{osc}$  decreases monotonically over time for extensional deformation. Analogously, Fig. 7 shows that  $E_{osc}$  increases monotonically over time for compressional deformation. Notice from Fig. 6 and Fig. 8 that the total energy of the system can either increase or decrease.

As described earlier, the value of  $E_{osc}$  over time can be obtained by integrating Eq. (16) throughout the course of deformation. This was done for the two example simulations above. The integrals were evaluating using an adaptive numerical integration scheme and the value of  $\frac{dF}{dt}$  was obtain from the sigmoid. The resulting curve for each simulation is plotted with numerical results shown in Fig. 5 and Fig. 7. From the plots it is clear that Eq. (16) can be used to obtain a basic approximation of  $E_{osc}(t)$  for this model.

The results of all simulations over the range of initial oscillation energies and strains shown in Fig. 9 extend the results of the previous studies.<sup>1,2</sup> Assuming small loads and small oscillation energies, these studies obtained a negative linear dependence of the oscillation energy on the deformation, which is compatible with the TEE. Fig. 9 shows the same result for small values of  $\epsilon_s$ , in addition to indicating features of the TEE for a larger range of oscillation energies and deformations. The negative slope in Fig. 9 demonstrates the TEE over the entire range of initial oscillation energies and strains. The different curves associated with each initial oscillation energy indicate the strength of the TEE depends on oscillation energy: For a given value of  $\epsilon_s$  (positive

or negative), the magnitude of  $\Delta E_{osc}/E_{osc_i}$  increases with  $E_{osc_i}$ , indicating that the strength of the TEE increases for larger values of  $E_{osc_i}$ . There also appears to be some asymmetry in strength of the TEE based on the direction of deformation: For  $E_{osc_i} = 10, 20,$  and  $30Kk_B$ , each curve has positive concavity, indicating that the TEE is stronger in compression than in tension for these cases. This is less clear for  $E_{osc_i} = 40Kk_B$ , since for this temperature the curve has negative concavity for positive strain. This may suggest that this asymmetry based on the direction of deformation is also oscillation energy dependent.

Fig. 10 indicates that the total energy can increase or decrease for this model. The quadratic curve corresponding  $E_{osc_i} = 10Kk_B$  is compatible with the previous studies. These explained that total energy decreases initially for extensional deformation since the approximate linear dependence of the oscillation energy (negative) dominates the higher order dependence of the potential energy (positive) for small strains. The inequality between these two energies reverses as the deformation increases, causing the total energy to increase for larger strains, as seen for  $E_{osc_i} = 10Kk_B$ . This trend seems to be limited to lower oscillation energies. For example, for  $E_{osc_i} = 40Kk_B$ ,  $\Delta E_{tot}/E_{tot_i}$  decreases up to  $\epsilon_s = 0.03$ , at which point the mass becomes unbounded from the well. One may be inclined to conclude that  $E_{osc}$  decreases for extensional simulations due to the initial decrease in  $E_{tot}$  for these simulations. However, it will be demonstrated for Model 2 that  $E_{osc}$  also decreases for extensional deformation despite that  $E_{tot}$  exclusively increases.

## B. Mechanism 2

It will be shown here that Mechanism 2 also contributes to the TEE. This mechanism was assessed by numerically evaluating Eq. (12) over a range of  $F$  and  $E_{osc}$ . A surface was fit to the data to yield the contour plot of  $\langle K \rangle / E_{osc}$  shown in Fig.

11. The upper right hand corner of the plot is omitted since this corresponds to values of  $E_{osc}$  that are unbounded for the given overall well. The dashed lines, which were determined from the simulation results of Mechanism 1, give the flow of  $E_{osc}$  throughout deformation. The orientation of the flow of  $E_{osc}$  relative to the contour plot indicates that this mechanism contributes to the TEE:  $\langle K \rangle / E_{osc}$  increases for compression and decreases for extension. This result is compatible with that obtained in a previous study.<sup>2</sup> Assuming small oscillation energies and deformations, the study obtained a negative linear relationship between  $\langle K \rangle$  and the strain, where  $\langle K \rangle / E_{osc}$  was slightly less than 0.5 for zero strain. This present study confirms this in addition to providing characteristics of this mechanism over a larger range of oscillation energy and deformation. The effect is stronger in tension than in compression, and this difference increases for increasing initial oscillation energy. For the maximum compressional strains,  $\langle K \rangle / E_{osc}$  changes by about 1% to 4% over the range of  $E_{osci}$ , and for the maximum extensional strains,  $\langle K \rangle / E_{osc}$  changes by about 10% to 30% over the range of  $E_{osci}$ . Comparing these results to that of Mechanism 1 (an approximate 40% change in  $\Delta E_{osc} / E_{osci}$  for maximum compressional strains and an approximate 30-35% change in  $\Delta E_{osc} / E_{osci}$  for maximum extensional strains), this mechanism should be considered for this model in addition to Mechanism 1 for extensional deformation, but it can be neglected for compressional strains.

## V. MODEL 2

The second model will now be considered. Before each mechanism is considered, some further details and restrictions concerning this model will now be outlined. Due to symmetry, the overall potential is given by  $U(r, t) = U_1(r) + U_2(r, t) = U_1(r) + U_1(c(t) - r)$ . The distance between the left and right atoms will be represented by  $c(t) = 2R + x_r(t)$ , where  $x_r$  is the position of the right atom. It is given by

$x_r = \Delta x_r + x_{r_e}$ , where  $\Delta x_r$  is the displacement of the mass from its initial position,  $x_{r_e}$ . This term represents the dynamic expansion of the bond. Dynamic expansion is the discrete analog of thermal expansion: oscillation energy present in a system of oscillators causes the system to expand beyond the size of the system with no energy. For this system, this causes the natural spacing between the left and right atoms, denoted as  $c_e$ , to be greater than  $2R$  for nonzero energy. Since  $x_{r_e}$  is included in  $x_r$  and does not affect the subsequent analysis, a quantitative description of dynamic expansion will be postponed until a discussion of verification simulations, were it becomes more relevant.

The following describes the imposed restrictions of this model. There is no restriction on  $E_{osc}$  since the well approaches infinity at both ends. It will be imposed that the deformation is such that a single minimum in the potential exists at the center of the well,  $c/2$ . Assuming each individual potential is Lennard-Jones, the only way a local maximum can be induced in the well is for extensional deformation above a critical value. Specifically, a local maximum will be induced at  $r = c/2$  if  $x_r/2 > (r_i - R)$ . Therefore, to ensure there is one minimum located at the center of the potential, it will be enforced that  $x_r/2 < (r_i - R)$ . When this is true, the mass oscillates symmetrically about the center of the well:  $r_r, r_l = c/2 \pm A$ , where  $A$  is the amplitude of oscillation.

## A. Mechanism 1

### 1. Analysis

Eq. (7) will now be applied to this model in a similar way to that of Model 1. Taking the partial derivative of  $U(r, t)$  with respect to time yields

$$\left. \frac{\partial U}{\partial t} \right|_{(r,t)} = \left. \frac{dU_1}{dr} \right|_{c(t)-r} \frac{dx_r}{dt}. \quad (30)$$

Substituting this expression into Eq. (7) with  $r_{min} = c/2$  yields

$$\frac{dE_{osc}}{dt} = \frac{dx_r}{dt} \left[ \frac{dU_1}{dr} \Big|_{c(t)-r(t)} - \frac{dU_1}{dr} \Big|_{c(t)/2} \right]. \quad (31)$$

The above equation will be averaged over time to compute to average value of  $\frac{dE_{osc}}{dt}$  at a given point in the deformation. For quasi-static deformation, it will be assumed that  $\frac{dx_r(t)}{dt} = v_r$  (i.e. constant over the course of deformation). Furthermore, since  $\left| \frac{dr}{dt} \right| \gg \left| \frac{dx_r}{dt} \right|$ , it will be assumed that  $c(t) = c$  over a period of oscillation of the mass. Taking into account the above approximations and averaging Eq. (31) over half of the period,  $T$ , yields

$$\left\langle \frac{dE_{osc}}{dt} \right\rangle_{c, E_{osc}} = v_r \left[ \frac{2}{T} \int_0^{T/2} \frac{dU_1}{dr} \Big|_{c-r(t)} dt - \frac{dU_1}{dr} \Big|_{c/2} \right]. \quad (32)$$

Converting to an integral over space yields

$$\left\langle \frac{dE_{osc}}{dt} \right\rangle_{c, E_{osc}} = v_r \frac{\int_{r_l^+}^{r_r^-} \left[ \frac{dU_1}{dr} \Big|_{c-r} - \frac{dU_1}{dr} \Big|_{c/2} \right] \frac{1}{\sqrt{K}} dr}{\int_{r_l^+}^{r_r^-} \frac{1}{\sqrt{K}} dr}. \quad (33)$$

A change of variables can be used to show that the above expression is equivalent to

$$\left\langle \frac{dE_{osc}}{dt} \right\rangle_{c, E_{osc}} = v_r \frac{\int_{r_l^+}^{r_r^-} \left[ \frac{dU_1}{dr} \Big|_r - \frac{dU_1}{dr} \Big|_{c/2} \right] \frac{1}{\sqrt{K}} dr}{\int_{r_l^+}^{r_r^-} \frac{1}{\sqrt{K}} dr}. \quad (34)$$

This equation has the same requirements as Eq. (16) for the existence of the TEE for this model. The integral in the numerator (denoted as  $I_2$ ) must be negative for the TEE to exist at the given value of  $c$  and  $E_{osc}$  (i.e., for the TEE to exist “locally”). For the TEE to exist for “globally”, it is necessary that  $I_2 < 0$  for all allowable values of  $c$  and  $E_{osc}$ . This will cause  $E_{osc}$  to increase and decrease monotonically for

compressional and extensional deformation, respectively, for any initial value of  $E_{osc}$ . This will now be demonstrated for the Lennard-Jones bond.

From symmetry,  $r_l = c - r_r$  and  $\frac{1}{\sqrt{K}}\Big|_r = \frac{1}{\sqrt{K}}\Big|_{c-r}$ . This allows  $I_2$  to be written as

$$I_2 = \int_{c/2}^{r_r^-} \left[ \frac{dU_1}{dr}\Big|_{c/2}^r + \frac{dU_1}{dr}\Big|_{c/2}^{c-r} \right] \frac{1}{\sqrt{K}}\Big|_r dr. \quad (35)$$

The following inequality can be justified in the same way as the analogous inequality in Model 1, simply by replacing  $r_{min}$  with  $c/2$ :

$$\frac{dU_1}{dr}\Big|_{c/2}^r = \int_{c/2}^r \frac{d^2 U_1}{dr^2} dr < \int_{c/2}^r \frac{d^2 U_1}{dr^2}\Big|_{c/2} dr = \frac{d^2 U_1}{dr^2}\Big|_{c/2} (r - c/2). \quad (36)$$

Substituting this result into Eq. (35) yields

$$I_2 = \int_{c/2}^{r_r^-} \left[ \frac{dU_1}{dr}\Big|_{c/2}^r + \frac{dU_1}{dr}\Big|_{c/2}^{c-r} \right] \frac{1}{\sqrt{K}}\Big|_r dr < \int_{c/2}^{r_r^-} \left[ \frac{d^2 U_1}{dr^2}\Big|_{c/2} (r - c/2) + \frac{d^2 U_1}{dr^2}\Big|_{c/2} (c/2 - r) \right] \frac{1}{\sqrt{K}}\Big|_r dr = 0. \quad (37)$$

Analogously to Model 1, this holds true for all allowable values of  $E_{osc}$  in addition to all values of  $c$  such that  $\frac{d^2 U_1}{dr^2}\Big|_{c/2} > 0$ , which is necessary for a minimum to exist in the center of the well. This implies that the TEE exists at all points over the course of deformation, meaning  $E_{osc}$  changes monotonically over deformation. This again was due to the softening of the Lennard-Jones potential.

## 2. Simulation

The analysis was verified via simulation in a similar manner to Model 1. The same parameter values corresponding to solid argon and initial oscillation energies were used. The values of strain, now defined as  $\Delta x_r/c_e$ , again ranged from -0.03 to 0.03. The quasi-static deformation was also modeled as a sigmoid given by a

fourth order polynomial. The value of  $x_r$  ranges from  $x_{r_e}$  to  $x_{r_e} + \Delta x_r$  over the interval  $[0, t_f]$ . The five constants were determined such that  $x_r(0) = x_{r_e}$ ,  $\dot{x}_r(0) = 0$ ,  $x_r(t_f/2) = \Delta x_r/2 + x_{r_e}$ ,  $x_r(t_f) = \Delta x_r + x_{r_e}$ , and  $\dot{x}_r(t_f) = 0$ . Quasi-static deformation was imposed by specifying  $\left(\frac{dx_r}{dt}\right)_{max} = \frac{dx_r}{dt}\Big|_{t_f/2} = 10^{-4}R/t_{osc}$ . Now  $t_{osc}$  is given by

$$t_{osc} = \frac{2\pi}{\sqrt{2k_{lin}/m}}, \quad (38)$$

where the factor of 2 is present since the atom is bound on each side. The maximum velocity of the right mass was conservatively approximated to be  $2\Delta x_r/t_f$ . The two expressions were equated to yield  $t_f = 2 \cdot 10^4 \Delta x_r t_{osc}/R$ .

Before the simulations could be carried out, a relationship was determined to calculate  $x_{r_e}$  in terms of  $E_{osc}$  for the system. The natural length of the three atom system,  $c_e$ , for a given value of  $E_{osc}$  is such that  $\langle F_l \rangle$ , the time average of the force exerted on the left fixed mass, is zero. Integrating the force over half of the period and converting the integral from time to space yields

$$\langle F_l \rangle = \int_{r_i^+}^{r_r^-} \frac{dU_1}{dr} \frac{1}{\sqrt{K}} dr = 0. \quad (39)$$

This equation was solved via an adaptive numerical integration method to determine the relationship between  $x_{r_e}$  and  $E_{osc}$ . The results are shown in Fig. 12. The data was fit with a sixth-order polynomial via unweighted least-squares linear regression. Notice that a similar process was not required for Model 1. Dynamic expansion is indeed present in Model 1 (i.e. the average position of the mass is to the right of the well bottom for nonzero oscillation energy), but it did not affect the simulation setup since the force  $F$  does not “start” anywhere, as was the case with the values of  $x_r$  here.

The equations of motion were again integrated using the fifth order Gear Predictor-Corrector integration scheme. The results of an extensional simulation and a compressional simulation demonstrating the TEE are shown in Fig. 13 to Fig. 16. Similar to Model 1,  $E_{osc}$  decreases monotonically over time for extension and increases for compression, shown in Fig. 13 and Fig. 15, respectively. Unlike Model 1, Fig. 14 and Fig. 16 indicate that the total energy of the system increases for both extensional and compressional deformation.

Analogously to Model 1, the value of  $E_{osc}$  over time was obtained for the two example simulations above by numerically evaluating Eq. (34) over the course of deformation. The resulting curve for each simulation is plotted on Fig. 13 and Fig. 15, which shows that Eq. (34) can be used to obtain a basic approximation of  $E_{osc}(t)$  for this model.

The results of all simulations over the ranges of initial temperatures and strains are shown in Fig. 17 and Fig. 18. The behavior of  $E_{osc}$  is overall similar to that of Model 1, where in both models  $\Delta E_{osc}/E_{osc_i}$  approximately ranges from -0.4 to 0.4. The negative slope in Fig. 17 demonstrates the TEE over the entire range of initial oscillation energies and strains. There does however appear to be some difference in the details of the effect between the two models. Unlike Model 1, the strength of the TEE here does not appear to be dependent on oscillation energy since the data points for different initial oscillation energies collapse onto the same curve. It should be emphasized that this conclusion is based on the way in which the strain was defined. The strain was defined in terms of  $c_e$ , not  $2R$ . This means that for  $E_{osc_{i1}} > E_{osc_{i2}}$ ,  $|\Delta x_{r1}| > |\Delta x_{r2}|$  for equivalent values of strain. This implies that if the strain was instead defined relative to  $2R$ , the strength of the TEE would decrease with  $E_{osc_i}$ , since for  $(\Delta E_{osc}/E_{osc_i})_1 = (\Delta E_{osc}/E_{osc_i})_2$ ,  $|\Delta x_{r1}| > |\Delta x_{r2}|$ . This trend is *opposite* to that of Model 1. From Fig. 17, the slight positive concavity of the curve

generated by the data points indicates that the TEE is stronger for compression than extensional deformation for all oscillation energies, which also differs from that observed in Model 1.

Unlike Model 1, Fig. 18 shows that the total energy increases for either compression or extension for this model. This shows that  $E_{osc}$ , a component of  $E_{tot}$ , can decrease despite an increase in  $E_{tot}$ .

### B. Mechanism 2

While Mechanism 2 contributed to the TEE in Model 1, this is not the case for this model. As with Model 1, this mechanism was assessed by numerically evaluating Eq. (12) over a range of  $x_r$  and  $E_{osc}$ . A surface was fit to the data to yield the contour plot of  $\langle K \rangle / E_{osc}$  shown in Fig. 19. The dashed lines, determined from the simulation results of Mechanism 1, give the flow of  $E_{osc}$  throughout deformation. From the orientation of these lines relative to the contour plot, it is clear that this mechanism does not contribute to the TEE:  $\langle K \rangle / E_{osc}$  increases for extensional deformation and decreases for compressional deformation. This shift in  $\langle K \rangle / E_{osc}$  therefore *counteracts* the TEE. However, its contribution is relatively small compared to that of Mechanism 1. For the maximum compressional strains,  $\langle K \rangle / E_{osc}$  changes by about 0.5% to 1% over the range of  $E_{osc_i}$ , and for the maximum extensional strains,  $\langle K \rangle / E_{osc}$  changes by about 1% to 2% over the range of  $E_{osc_i}$ . These are relatively small compared to the approximate 30% change in  $\Delta E_{osc} / E_{osc_i}$  for maximum extensional strain and to the approximate 35% change in  $\Delta E_{osc} / E_{osc_i}$  for maximum compressional strain. As such, this mechanism can be neglected in assessing the TEE for this model.

## VI. CONCLUSION

In summary, this study has considered the deformation of a one atom system in order to assess the causes of the TEE. It utilized two models of such a system and

considered two possible causes of the TEE, denoted as Mechanism 1 and Mechanism 2, for each model. To assess Mechanism 1, the Lennard-Jones potential was applied to a general expression for  $\langle \frac{dE_{osc}}{dt} \rangle$ . It was shown for each model that  $\langle \frac{dE_{osc}}{dt} \rangle > 0$  and  $\langle \frac{dE_{osc}}{dt} \rangle < 0$  for compressional and extensional deformation, respectively, thus demonstrating compatibility with the TEE. Numerical simulation was used to verify the results of this analysis and to assess properties of the TEE over a range of oscillation energies and deformations. The characteristics of  $\Delta E_{osc}/E_{osci}$  were similar in each model with some minor differences. The results for the previously studied model, Model 1, were compatible with the results of the previous studies. To assess Mechanism 2, an expression for  $\langle K \rangle$  for the Lennard-Jones potential was numerically evaluated over a range of oscillation energies and deformations. Unlike Mechanism 1, the results were fundamentally different between the two models. For Model 1, the change in  $\langle K \rangle / E_{osc}$  throughout deformation was compatible with the TEE, while for Model 2 it was not. The results for Model 1 were compatible with those of a previous study. With the exception of extensional deformation for Model 1, the effect of this mechanism was about an order of magnitude smaller than that of Mechanism 1.

The compatibility of Mechanism 1 with the TEE for both models and the difference of Mechanism 2 between the two models suggests that Mechanism 1 should be considered the primary mechanism of the TEE. Recalling the analysis of Mechanism 1, the “bond softening” of the Lennard-Jones potential should be considered the primary cause of the TEE. The goal of a subsequent study is to extend these results to a multiple atom system.

## ACKNOWLEDGMENTS

M.K. thanks the Notre Dame Energy Center for a Vincent P. Slatt Fellowship.

## Notes

<sup>1</sup>Notice for this interval that  $\int_r^{r_{min}} \frac{d^2 U_1}{dr^2} dr > \int_r^{r_{min}} \frac{d^2 U_1}{dr^2} \Big|_{r_{min}} dr$ . Negating each side and flipping the limits of integration yields the inequality in Eq. (19).

<sup>2</sup>The exception is after the minimum concavity is reached, when the concavity begins to increase asymptotically towards zero. However, because the center of oscillation is at positive concavity, this had no effect.

<sup>3</sup>The temperature for a single atom system is not defined.

<sup>4</sup>In an earlier study,<sup>5</sup> the range of fractional volumetric strain for solid argon used was  $V/V_0 = [0.9, 1.1]$ . The linear strain was approximated from this by taking the cube root, which approximately yields the range  $\epsilon_s = [-0.03, 0.03]$ .

## References

- [1] V. L. Gilyarov, A. I. Slutsker, V. P. Volodin, and L. A. Laius. Energetics of an adiabatically-loaded excited anharmonic oscillator. *Physics of the Solid State*, 1997.
- [2] A. I. Slutsker, V. L. Gilyarov, and A. S. Luk'yanenko. Energy features of an adiabatically loaded anharmonic oscillator. *Physics of the Solid State*, 2006.
- [3] B. Schweizer and J. Wauer. Atomistic explanation of the gough-joule-effect. *The European Physical Journal*, 2001.
- [4] Alessandro Cuccoli, Alessandro Macchi, and Valerio Tognetti. Monte carlo computations of the quantum kinetic energy of rare-gas solids. *Physical Review*, 1993.
- [5] Somnath Bhowmick and Vijay B. Shenoy. Effect of strain on the thermal conductivity of solids. *The Journal of Chemical Physics*, 2006.

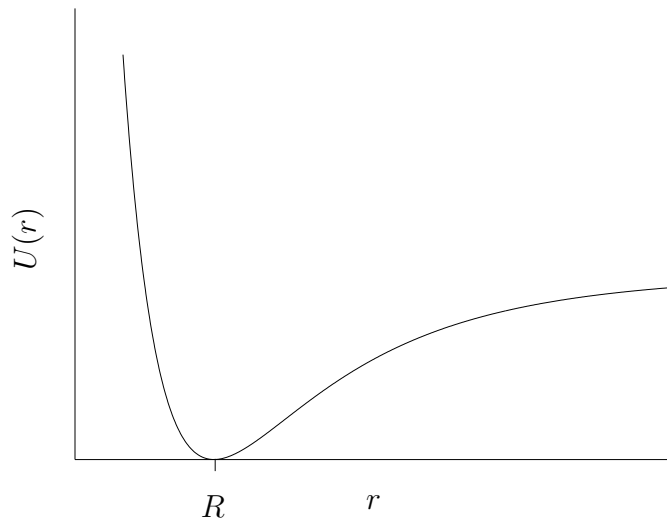


FIG. 1. The Lennard-Jones interatomic potential.

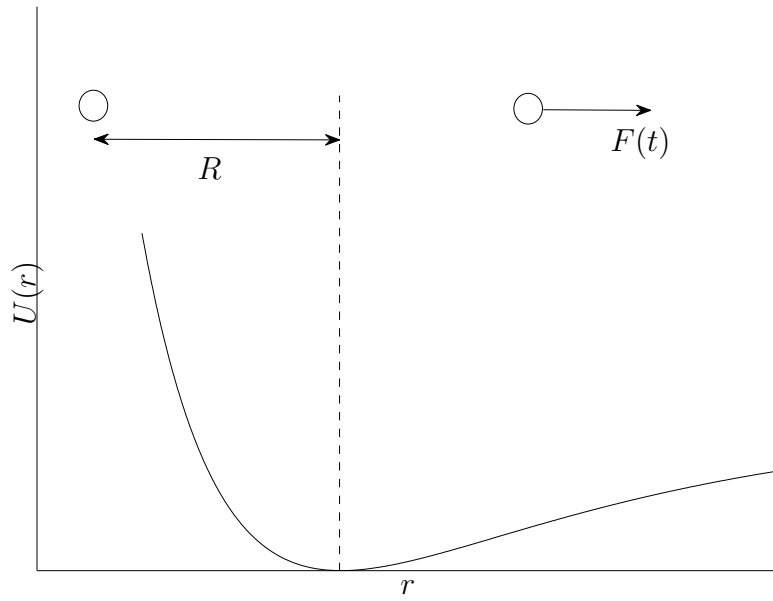


FIG. 2. The first model of deformation of an atomic oscillator, referred to as Model 1.

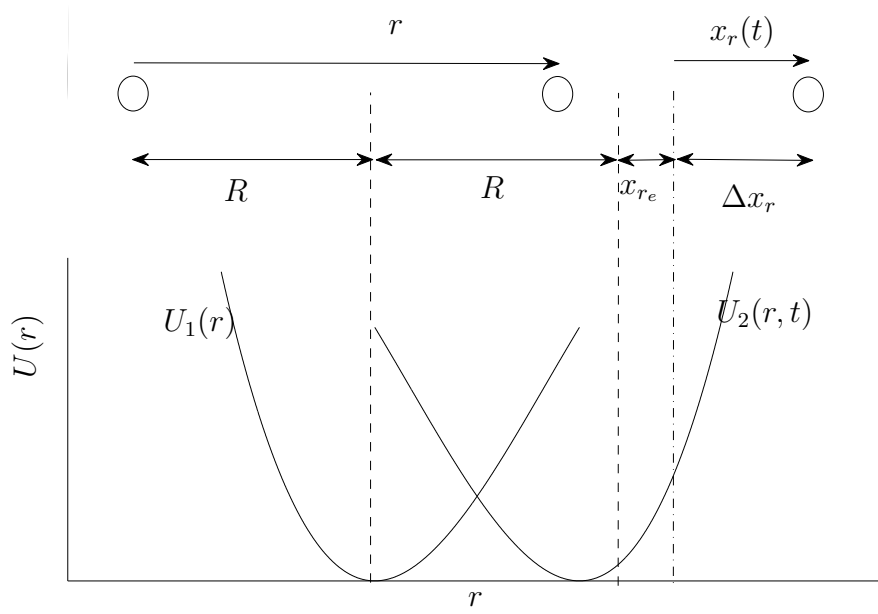


FIG. 3. The second model of deformation of an atomic oscillator, referred to as Model 2.

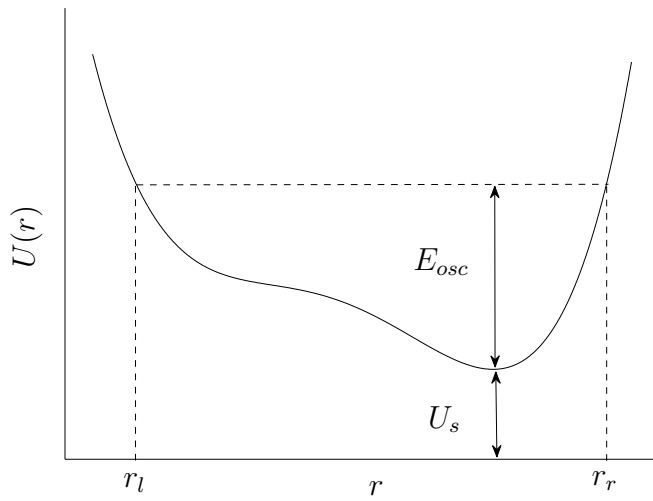


FIG. 4. A general potential well with a static potential energy  $U_s$ . An oscillator with an oscillation energy  $E_{osc}$  is bound in the well.

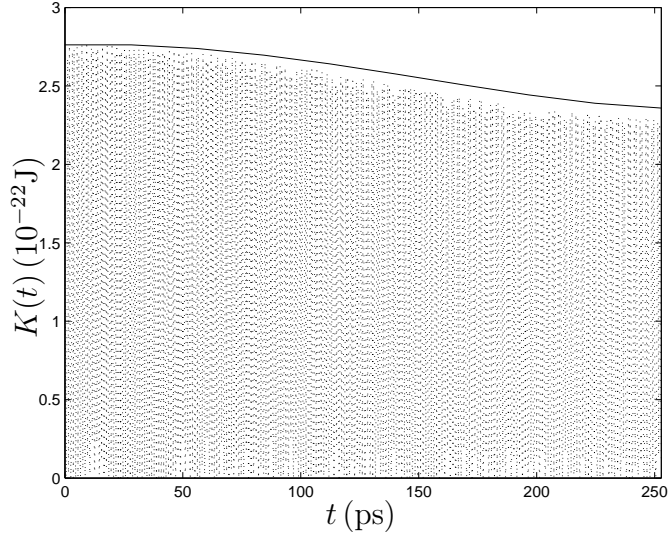


FIG. 5. Plot of  $K(t)$  vs  $t$  for  $E_{osc_i} = 20Kk_B$  and  $\epsilon_s = 0.015$  for Model 1. The maximum value of  $K$  at a given  $t$  corresponds to  $E_{osc}$  at that time. The solid curve was obtained by numerically integrating Eq. (16).

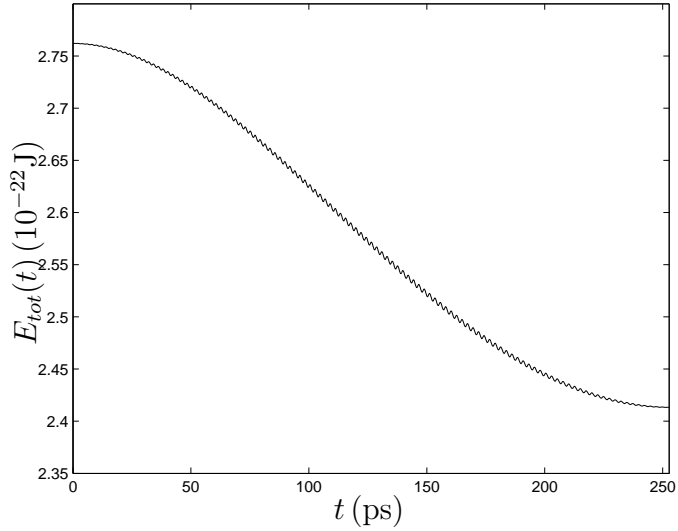


FIG. 6. Plot of  $E_{tot}(t)$  vs  $t$  for  $E_{osc_i} = 20Kk_B$  and  $\epsilon_s = 0.015$  for Model 1.

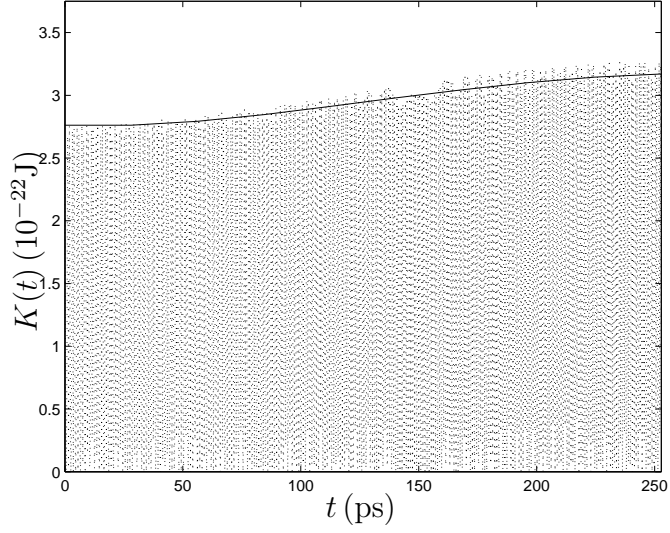


FIG. 7. Plot of  $K(t)$  vs  $t$  for  $E_{osc_i} = 20Kk_B$  and  $\epsilon_s = -0.015$  for Model 1. The maximum value at a given  $t$  corresponds to  $E_{osc}$  at that time. The solid curve was obtained by numerically integrating Eq. (16).

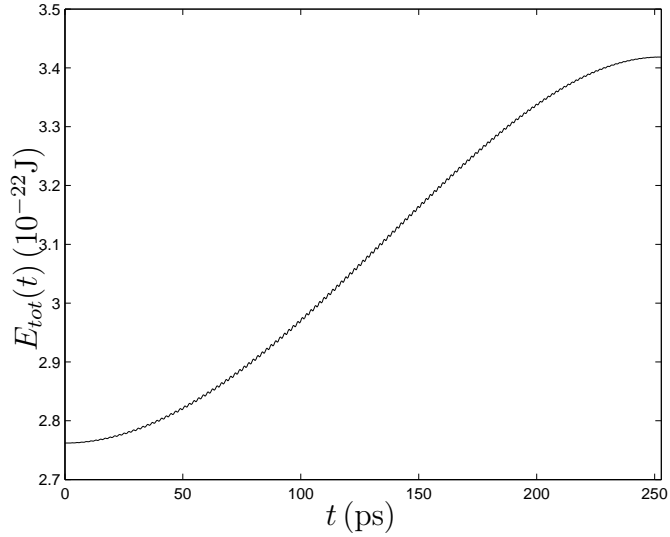


FIG. 8. Plot of  $E_{tot}(t)$  vs  $t$  for  $E_{osc_i} = 20Kk_B$  and  $\epsilon_s = -0.015$  for Model 1.

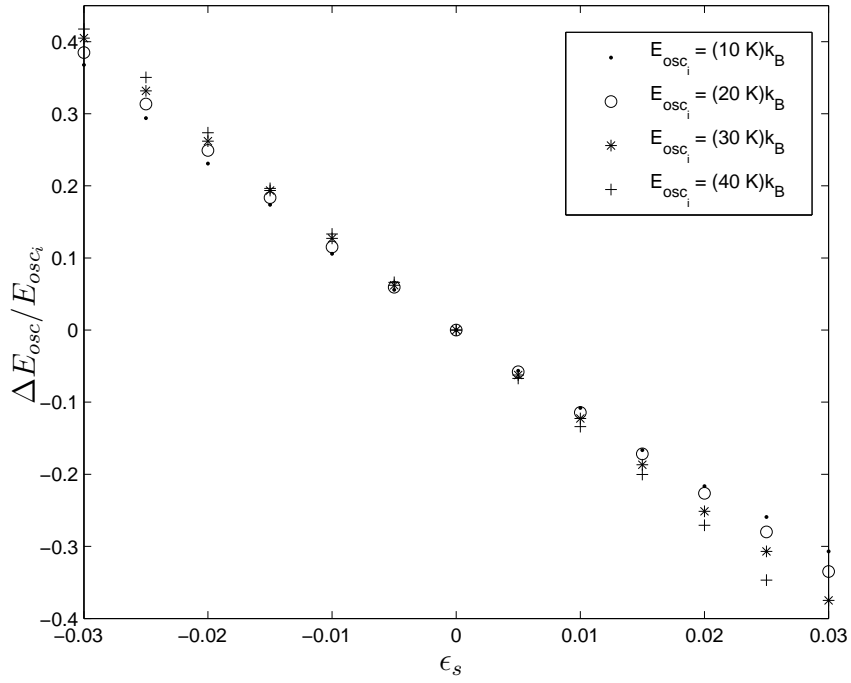


FIG. 9. Plot of  $\Delta E_{osc}/E_{osc_i}$  vs  $\epsilon_s$  for a range of initial oscillation energies for Model 1.

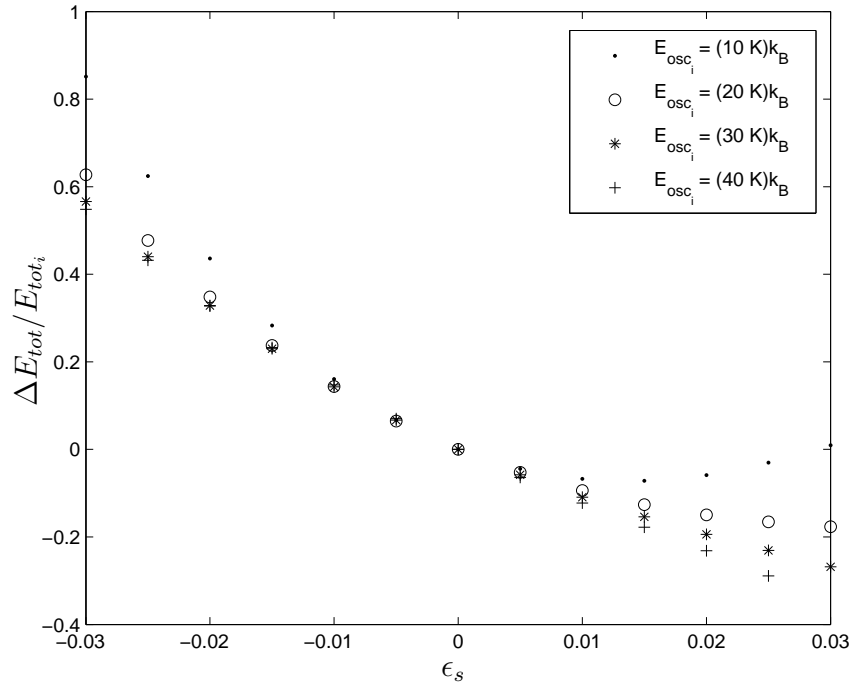


FIG. 10. Plot of  $\Delta E_{tot}/E_{tot_i}$  vs  $\epsilon_s$  for a range of initial oscillation energies for Model 1.

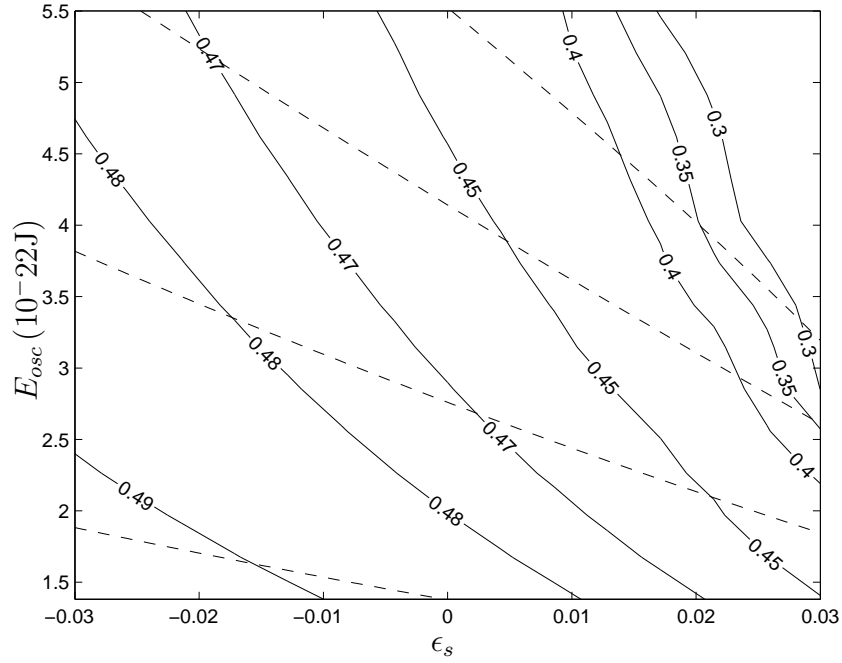


FIG. 11. Contour plot of  $\langle K \rangle / E_{osc}$  over a range of  $\epsilon_s$  and  $E_{osc}$  for Model 1. The dashed lines, which were determined from the simulation results of Mechanism 1, give the flow of  $E_{osc}$  throughout deformation.

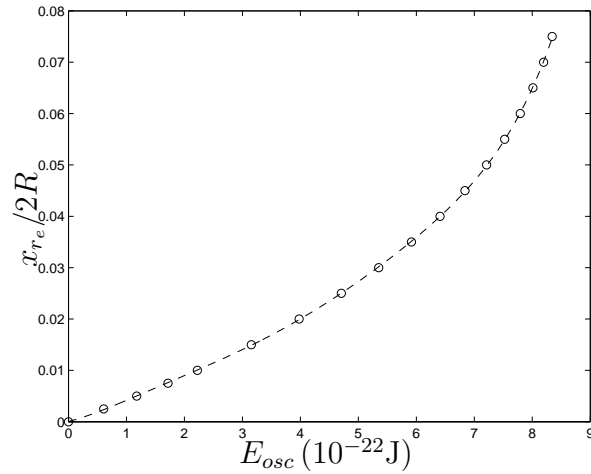


FIG. 12. Dynamic expansion for Model 2 over a range of values of  $E_{osc}$ .

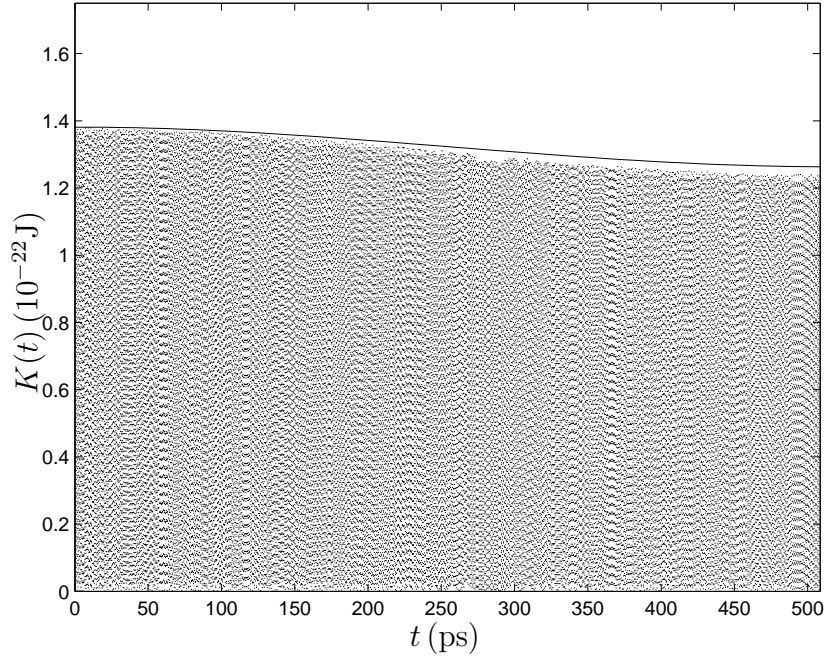


FIG. 13. Plot of  $K(t)$  vs  $t$  for  $E_{osc_i} = 10Kk_B$  and  $\Delta x_r = 0.01c_e$  for Model 2. The maximum value at a given  $t$  corresponds to  $E_{osc}$  at that time. The solid curve was obtained by numerically evaluating Eq. (34).

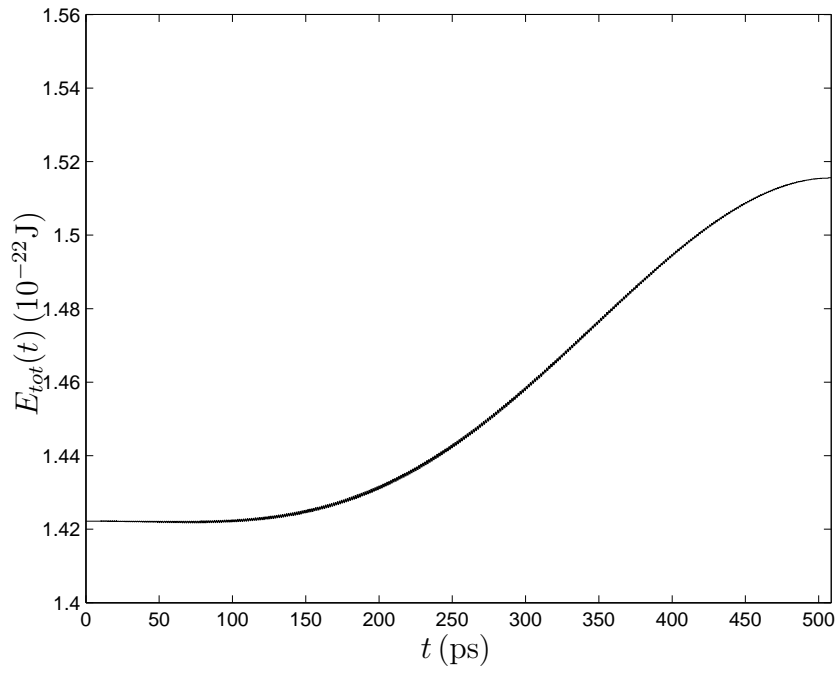


FIG. 14. Plot of  $E_{tot}(t)$  vs  $t$  for  $E_{osc_i} = 10Kk_B$  and  $\Delta x_r = 0.01c_e$  for Model 2.

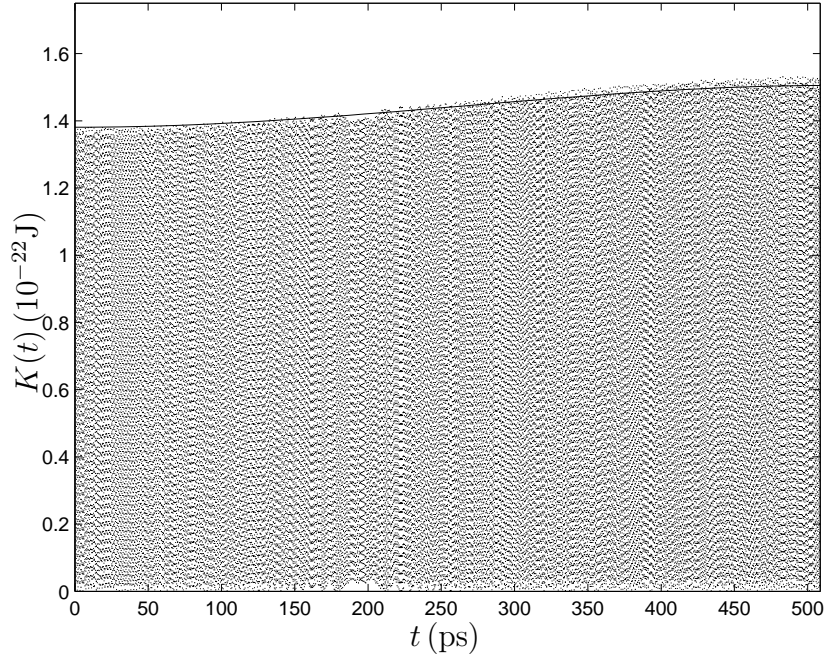


FIG. 15. Plot of  $K(t)$  vs  $t$  for  $E_{osc_i} = 10Kk_B$  and  $\Delta x_r = -0.01c_e$  for Model 2. The maximum value at a given  $t$  corresponds to  $E_{osc}$  at that time. The solid curve was obtained by numerically evaluating Eq. (34).

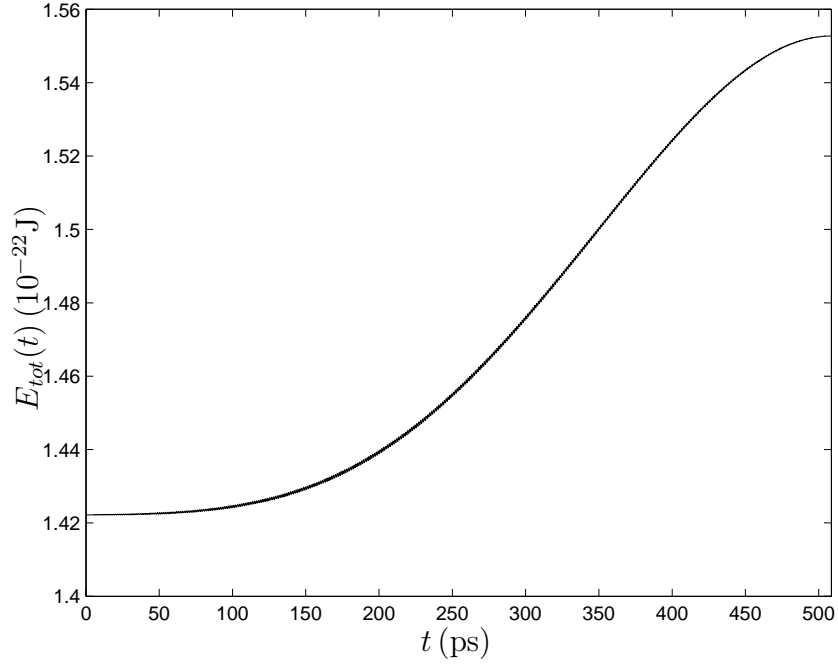


FIG. 16. Plot of  $E_{tot}(t)$  vs  $t$  for  $E_{osc_i} = 10Kk_B$  and  $\Delta x_r = -0.01c_e$  for Model 2.

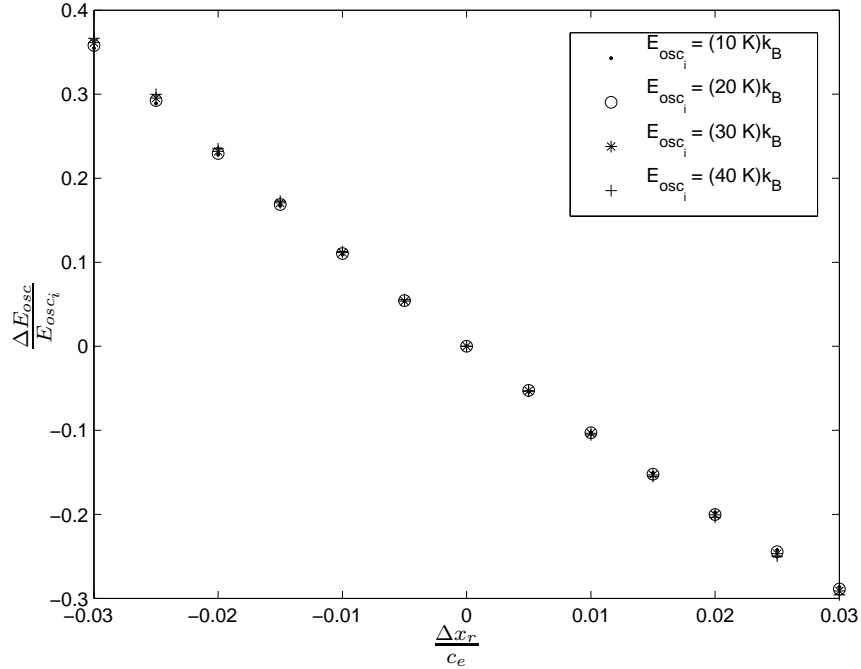


FIG. 17. Plot of  $\frac{\Delta E_{osc}}{E_{osc_i}}$  vs  $\frac{\Delta x_r}{c_e}$  over a range of initial oscillation energies for Model 2.

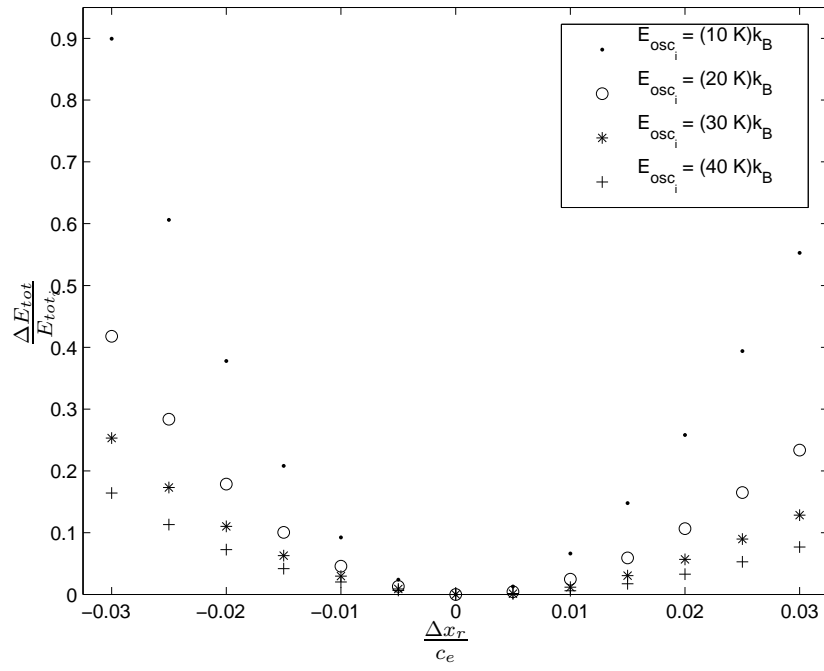


FIG. 18. Plot of  $\frac{\Delta E_{tot}}{E_{tot_i}}$  vs  $\frac{\Delta x_r}{c_e}$  over a range of oscillation energies for Model 2.

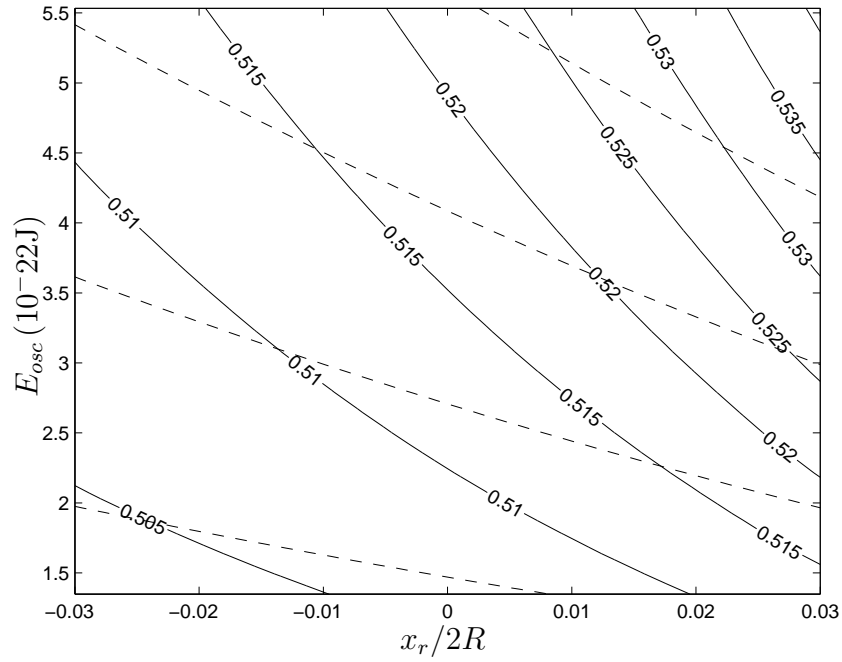


FIG. 19. Contour plot of  $\langle K \rangle / E_{osc}$  over a range of  $x_r$  and  $E_{osc}$  for Model 2. The dashed lines, which were determined from the simulation results of Mechanism 1, give the flow of  $E_{osc}$  throughout deformation.